Journal of Information Systems Engineering and Management
2025, 10(28s)
e-ISSN: 2468-4376
https://www.jisem-journal.com/

Research Article

Mathematical Modeling and Simulation of High-Speed Solid Rotor Induction Motor

Abdullah Maya Fazaa[1] and Ahmed Thamer Radhi[2]

[1]Electrical Engineering Department, University of Misan, Misan, Iraq

[2]Electromechanical Eng. Dept., Engineering Technical College of Missan, Southern Technical University, Basrah, Iraq
*Corresponding author E-mail: enghre.2205@uomisan.edu.iq

ARTICLE INFO

Received: 23 Dec 2024

Revised: 23 Feb 2025

Accepted:28 Feb 2025

ABSTRACT

This study presents a comprehensive mathematical modeling and simulation of a high-speed solid rotor induction motor (HS-SRIM), focusing on the derivation of rotor impedance and the implementation of a dq-axis model for dynamic performance analysis. The research addresses the inherent challenges of solid rotor designs, including elevated electromagnetic losses and nonlinear material behavior, while highlighting their mechanical robustness and suitability for high-speed applications. Utilizing equivalent electrical circuits (EECs) and dq-axis transformations, the rotor impedance is analytically derived, incorporating factors such as edge effects, rotor saturation, and slip-dependent parameters. A MATLAB/Simulink model is developed to simulate the motor's transient and steady-state behavior under varying loads, with and without edge effect corrections. Key results demonstrate the impact of edge effects on torque, current, speed, and power characteristics, revealing significant performance deviations between idealized and practical rotor configurations. The simulation validates the model's accuracy in capturing high-speed dynamics at 400 Hz, though it underscores limitations in efficiency at elevated frequencies.

Keywords: configurations, dynamics, underscores, characteristics

1. INTRODUCTION

Solid rotor induction motors (SRIMs) are extensively employed in applications requiring heavy-load starting, frequent braking, flywheel energy storage, gas compressors, and other high-speed operational environments[1] [2]. In contrast to laminated rotors, solid rotors offer structural simplicity, enhanced mechanical robustness, improved startup performance, greater operational reliability, and reduced vibration and acoustic noise. However, these benefits are accompanied by elevated electromagnetic losses. Contemporary approaches to mitigating rotor losses involve structural modifications, such as introducing slots or incorporating squirrel cage configurations. These optimizations, while effective for loss reduction, may compromise the rotor's mechanical integrity. Consequently, rotor design must be tailored to specific application demands[3]. Despite these trade-offs, the smooth solid rotor remains a foundational element in SRIM research, playing a pivotal role in advancing optimization strategies and broadening the adoption of SRIM technology

Despite considerable academic exploration, solid-rotor induction motors (SRIMs) garnered minimal interest from the electrical machine industry between 1950 and 1980. A resurgence of SRIM research emerged in the 1990s, driven by advancements in high-speed technology [4] Recent attention to machines featuring alternating electromagnetic fields in solid ferromagnetic components stems from novel applications, including high-speed direct-drive compressors, pump and drill motors, superconducting systems, high-speed generators, and bearingless machines[5][6] . Over the past two decades, significant research on high-speed SRIMs has been conducted at institutions such as the Swiss Federal Institute of Technology in Zurich [7], Helsinki University of Technology[8] , and Lappeenranta University of Technology [9]

When compared to cage-rotor induction motors of equivalent dimensions, SRIMs exhibit reduced output power, lower power factor and efficiency, higher no-load slip, and elevated mechanical time constant[10].

Performance improvements in SRIMs can be achieved by reducing rotor impedance through strategies such as:

Selecting solid materials with a low ratio of relative magnetic permeability to electrical conductivity (μ_k/σ) while maintaining sufficient tensile strength.

Implementing layered (sandwiched) rotors combining materials with high magnetic permeability and conductivity.

Incorporating auxiliary cage windings or axial/radial slits into the solid rotor design.

2.ELECTROMAGNETIC THEORY

Analytical design methodologies for solid-rotor induction motors (SRIMs) traditionally involve substantial simplifications of machine behavior. Historically, analytical approaches assumed an unsaturated rotor with constant permeability, resulting in significant discrepancies between modeled and experimentally measured machine behavior [11]. Subsequent efforts to improve accuracy incorporated 3D modeling of solid-rotor geometries, better aligning analytical predictions with empirical data[11] . Contemporary analytical frameworks now account for rotor saturation [12], with advanced techniques segmenting the rotor into discrete layers for refined analysis. For example, ref [11] integrates three-dimensional linear methods with transfer matrix theory, achieving improved accuracy at the cost of increased complexity, albeit limited to smooth solid rotors (SSRs). Recent advancements[13] focus on enhancing analytical precision, though these methods remain restricted to SSRs.

Simpler and more adaptable alternatives, such as equivalent electrical circuits (EECs), have gained traction for steady-state performance evaluation due to their computational simplicity. Modern iterations, including T-shaped EECs [49, 87], leverage empirical formulations to optimize parameter estimation.. Here , d-q axis modeling will be used to characterize machine dynamics..

2.1. Equivalent circuit and rotor impedance

The operational principles of high-speed solid-rotor induction motors are analogous to those of conventional induction motors; however, significant analytical challenges arise due to the inherent nonlinearity of ferromagnetic rotor materials and the structural complexity inherent to certain solid-rotor designs. While the stator rotating magnetic field can be approximated as two-dimensional (2-D), the electromagnetic field within the solid rotor exhibits pronounced three-dimensional (3-D) characteristics. By analyzing the 2-D electromagnetic field distribution within the machine, the rotor impedance under fundamental field conditions and balanced three-phase operation has been derived. Incorporating the nonlinear characteristics of ferromagnetic rotor materials, the complex propagation constant is expressed [14]as

$$\alpha_{Fe} = \sqrt{jw\mu_o\mu_{rs}\sigma_{Fe}} = (a_R + ja_x)k_{Fe} \quad (1)$$

Where w is the angular frequency (rad/s), μ_o is the free space magnetic permeability (H/m), μ_{rs} is the relative magnetic permeability of surface (H/m), σ_{Fe} is the conductivity of rotor (S/m), a_R is the resistance coefficient for including hysteresis losses and nonlinear magnetic permeability, a_x is the reactance coefficient for including hysteresis losses and nonlinear magnetic permeability and k_{Fe} is the electromagnetic field attenuation coefficient (1/m).

The conductive medium attenuation coefficient with its conductivity and magnetic permeability is given by:

$$k_{Fe} = \sqrt{\frac{w\mu_o\mu_{rs}\sigma_{Fe}}{2}} \quad (2)$$

The rotor impedance has been derived for fundamental field and balanced three-phase system is given by[14]:

$$Z_r = \frac{jw\mu_{Fe}}{k_{Fe}}\frac{L}{\tau} = \frac{jw\mu_{Fe}\sigma_{Fe}}{k_{Fe}\sigma_{Fe}}\frac{L}{\tau} \approx \frac{\alpha_{Fe}}{\sigma_{Fe}}\frac{L}{\tau}$$

Where L is the rotor length (m) and τ is the pole pitch (m). Substituting (1) and (2) into (3), respectively, the new expression of Zr is equal to:

$$Z_r = (a_R + ja_x)\frac{L}{\tau}\sqrt{\frac{w\mu_o\mu_{rs}}{2\sigma_{Fe}}}$$

The angular frequency of rotor $w = 2\pi f_r$, where f_r is the rotor frequency (Hz), for rotating field of positive sequence $f_r^+ = sf$ and for rotating field of negative sequence $f_r^- = (2-s)f$, substituting into (4), yields:

$$Z_r = (a_R + ja_x)\frac{L}{\tau}\sqrt{\frac{\pi f_r\mu_o\mu_{rs}}{\sigma_{Fe}}} \quad (5)$$

To include the edge effect, solid steel conductivity σ_{Fe} in k_{Fe} parameter must be multiplied with the square of edge factor reciprocal k_z :

$$\sigma_{Fe} = \frac{\sigma_{Fe}}{k_z{}^2} \tag{6}$$

where $k_z = 1 + \frac{2}{\pi}\frac{\tau}{L}$

substituting (6) into (5), yields:

$$Z_r = (a_R + jax_x)k_z \frac{L}{\tau}\sqrt{\frac{\pi f_r \mu_o \mu_{rs}}{\sigma_{Fe}}} \tag{7}$$

Stator referred rotor impedance is obtained by multiplying the impedance given in (7) by the transformation coefficient k_t is given by:

$$k_t = \frac{2\, m_1 (N_1 k_{w1})^2}{p} \tag{8}$$

Where m_1 is the stator phases number, N_1 is the number of turn per phase of stator, k_{w1} is the stator winding factor and p is the pole pairs number.

The referred to the stator rotor impedance is given by:

$$Z_r' = (a_R + ja_x)k_t k_z \frac{L}{\tau}\sqrt{\frac{\pi f \mu_o \mu_{rs}}{\sigma_{Fe}}} \quad (9)$$

For positive sequence rotating field $f_r^+ = sf$, proposed stator referred rotor impedance is given by:

$$Z_{r+}' = (a_R + ja_x)k_t k_z \frac{L}{\tau}\sqrt{\frac{\pi sf \mu_o \mu_{rs}}{\sigma_{Fe}}} \quad (10)$$

$$R_{r+}' = a_R k_t k_z \frac{L}{\tau}\sqrt{\frac{\pi sf \mu_o \mu_{rs}}{\sigma_{Fe}}} = a_R Z_c \sqrt{\mu_{rs}}\sqrt{s} \quad (11)$$

$$X_{r+}' = a_X k_t k_z \frac{L}{\tau}\sqrt{\frac{\pi s f \mu_o \mu_{rs}}{\sigma_{Fe}}} = a_X Z_c \sqrt{\mu_{rs}}\sqrt{s} \quad (12)$$

For negative sequence rotating field $f_r^- = (2 - s)f$, proposed rotor impedance referred to stator is given by:

$$Z_{r-}' = (a_R + ja_x)k_t k_z \frac{L}{\tau}\sqrt{\frac{\pi(2-s) f \mu_o \mu_{rs}}{\sigma_{Fe}}} \tag{13}$$

$$R_{r-}' = a_R k_t k_z \frac{L}{\tau}\sqrt{\frac{\pi(2-s) f \mu_o \mu_{rs}}{\sigma_{Fe}}} = a_R Z_c \sqrt{\mu_{rs}}\sqrt{2-s} \tag{14}$$

$$X_{r-}' = a_X k_t k_z \frac{L}{\tau}\sqrt{\frac{\pi(2-s) f_o \mu_{rs}}{\sigma_{Fe}}} = a_X Z_c \sqrt{\mu_{rs}}\sqrt{2-s} \tag{15}$$

where $Z_c = k_t k_z \frac{L}{\tau}\sqrt{\frac{\pi f \mu_o}{\sigma_{Fe}}}$ is the rotor impedance constant value which is independent on the values of slip s and the surface relative magnetic permeability μ_{rs}.

where

$$R_2' = \frac{R_{2s}'}{s} = a_R Z_c \sqrt{\frac{\mu_{rs}}{s}} \tag{16}$$

$$X_2' = \frac{X_{2s}'}{s} = a_R Z_c \sqrt{\frac{\mu_{rs}}{s}} \tag{17}$$

are the resistance and reactance in the rotor branch of the equivalent circuit referred to the stator system. Fig. 18 shows the development of the equivalent circuit (transformer analogy) of a solid-rotor induction motor.

the equivalent circuit for a solid-rotor induction motor should be developed and how the resistance and reactance of the rotor branch vary with the slip[15], . This will be used in dq-model

3. DQ MODEL AND MATLAB SIMULATION

The dq model transforms the three-phase currents and voltages into two orthogonal components (direct and quadrature) which simplifies the analysis of the motor's dynamic performance.

solid rotor induction motor needs Values for Rs , Xs , R2 , X m and X2 to be modeled in addition to the governor equations.to make the usual modeling equations applicable to a machine with solid, round rotor, a circuit (denoted by subscript g) will be assumed present on the quadrature axis of the rotor. This new circuit is analogous to the main field winding (denoted by f) on the direct axis of the rotor(kimbark111) [16]

Ld and Lq for stator needs first to find the magnetizing inductances Md and Mq,, these inductances assumed to be equal in this machine , denote M for both Md and Mq will ease the steps .

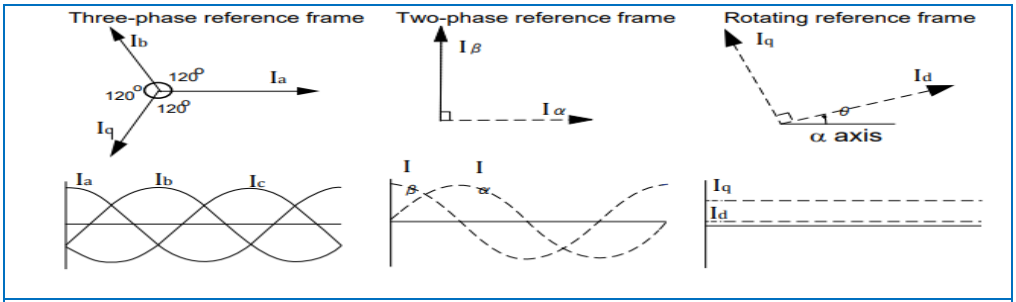

Fig. 8 the three reference frames

Clarke Transformation
Balanced three-phase quantities are transformed into balanced two-phase quadrature quantities by this process.
Park Transformation
Vectors in a balanced two-phase orthogonal stationary system are transformed into an orthogonal rotating reference frame using this transformation.
In essence, this implementation takes into account three reference frames:
1. A three-phase reference frame with co-planar three-phase quantities Ia, Ib, and Ic positioned at a 120-degree angle to one another.
2. Orthogonal stationary reference frame: this frame is in the same plane as the three-phase reference frame, but Iα (along the α axis) and Iβ (along the β axis) are perpendicular to one another.
3. An orthogonal rotating reference frame, where Iq is perpendicular to Id along the q axis and Id is at an angle θ (rotation angle) to the α axis. Figure 1 shows the three reference frames

The relationship between αβ and abc is as follows[17]:

$$\begin{bmatrix} V_\alpha \\ V_\beta \end{bmatrix} = \frac{2}{3}\begin{bmatrix} 1 & \frac{1}{2} & -\frac{1}{2} \\ 0 & \frac{\sqrt{3}}{2} & -\frac{\sqrt{3}}{2} \end{bmatrix}\begin{bmatrix} V_a \\ V_b \\ V_c \end{bmatrix} \qquad (18)$$

Then, the direct and quadrature axes voltages are:

$$\begin{bmatrix} V_d \\ V_q \end{bmatrix} = \begin{bmatrix} \cos\theta & \sin\theta \\ -\sin\theta & \cos\theta \end{bmatrix}\begin{bmatrix} V_\alpha \\ V_\beta \end{bmatrix} \qquad (19)$$

$$\begin{bmatrix} i_\alpha \\ i_\beta \end{bmatrix} = \begin{bmatrix} \cos\theta & -\sin\theta \\ \sin\theta & \cos\theta \end{bmatrix}\begin{bmatrix} i_d \\ i_q \end{bmatrix} \qquad (20)$$

The instantaneous values of the stator and rotor currents in three-phase system are ultimately calculated using the following transformation;

$$\begin{bmatrix} i_a \\ i_b \\ i_c \end{bmatrix} = \frac{2}{3}\begin{bmatrix} 1 & 0 \\ -\frac{1}{2} & -\frac{\sqrt{3}}{2} \\ -\frac{1}{2} & -\frac{\sqrt{3}}{2} \end{bmatrix}\begin{bmatrix} i_\alpha \\ i_\beta \end{bmatrix} \qquad (21)$$

If L_m is usual magnetizing inductance , its equal in each phase and it can be caliculated as[18]

$$L_m = \mu_0 \frac{2m\tau_p}{p\pi^2 g} l'(k_w N)^2 \qquad (22)$$

Lr is rotor equivilent inductance

Ld is the direct-axis synchronous inductance.

Lq is the quadrature-axis synchronous inductance.

the machine's stator and rotor synchronouse inductance are:

$$Ld = Lq = L_{\mathrm{s}} = L_{\mathrm{m}} + L_{\mathrm{ls}} \quad (23)$$

$$Lf = Lg = L_{\mathrm{r}} = L_{\mathrm{m}} + \frac{L_{\mathrm{lr}}}{s} \quad (24)$$

$$L_{md} = L_{mq} = L_m \quad (25)$$

$$\lambda_d = L_d i_d + L_{m_f} i_f \quad (26)$$

$$\lambda_q = L_q i_q + L_{m_g} i_g \quad (27)$$

$$\lambda_f = L_{ff} i f_f + L_{m_f} i_d \quad (28)$$

$$\lambda_g = L_{gg} i_g + L_{m_g} i_q \quad (29)$$

$$v_d = r i_d + \frac{d\lambda_d}{dt} + \omega\lambda_q \quad (30)$$

$$v_q = r i_q + \frac{d\lambda_q}{dt} - \omega\lambda_d \quad (31)$$

$$v_f = R_f i_f + \frac{\mathrm{d}}{\mathrm{d}t}\lambda_g + (\omega - \omega r)\lambda_g \quad (32)$$

$$v_g = R_g i_g + \frac{\mathrm{d}}{\mathrm{d}t}\lambda_f - (\omega - \omega r)\lambda_f \quad (33)$$

$$\frac{di_{\mathrm{d}}}{dt} = \frac{1}{Ls}\left(v_d - r i_{\mathrm{d}} - L_m \frac{di_{\mathrm{f}}}{dt} - \omega L_m i_{\mathrm{g}} - \omega L_q i_{\mathrm{q}}\right) \quad (34)$$

$$\frac{di_{\mathrm{q}}}{dt} = \frac{1}{Ls}\left(V_q - r i_{\mathrm{q}} - L_m \frac{di_{\mathrm{g}}}{dt} + \omega L_m i_{\mathrm{f}} + \omega L d i_{\mathrm{d}}\right) \quad (35)$$

$$\frac{di_{\mathrm{g}}}{dt} = \frac{1}{L_r}\left(\mathrm{o} - rf i_{\mathrm{f}} - \frac{3}{2} L_m \frac{di_{\mathrm{d}}}{dt} + (\omega - \omega r)\lambda_f\right) \quad (36)$$

$$\frac{di_{\mathrm{f}}}{dt} = \frac{1}{Ls}\left(\mathrm{o} - r_g i_g - \frac{3}{2} L_m \frac{di_{\mathrm{q}}}{dt} - (\omega - \omega r)\lambda_g\right) \quad (37)$$

$$id = \int \frac{1}{Ls}\left(v_d - r i_{\mathrm{d}} - L_m \frac{di_{\mathrm{f}}}{dt} - \omega L_m i_{\mathrm{g}} - \omega L_q i_{\mathrm{q}}\right) \quad (38)$$

$$i_{\mathrm{q}} = \int \frac{1}{Ls}\left(V_q - r i_{\mathrm{q}} - L_m \frac{di_{\mathrm{g}}}{dt} + \omega L_m i_{\mathrm{f}} + \omega L d i_{\mathrm{d}}\right) \quad (39)$$

$$i_g = \int \frac{1}{L_r}\left(\mathrm{o} - rf i_{\mathrm{f}} - \frac{3}{2} L_m \frac{di_{\mathrm{d}}}{dt} + (\omega - \omega r)\lambda_f\right) \quad (40)$$

$$i_{\mathrm{f}} = \int \frac{1}{\mathrm{Lr}}\left(\mathrm{o} - r_g i_g - \frac{3}{2} L_m \frac{di_{\mathrm{q}}}{dt} - (\omega - \omega r)\lambda_g\right) \quad (41)$$

$$T_e = \frac{3}{2}\left(\frac{P}{2}\right)\left(\Psi_f i_g - \Psi_g i_f\right) \quad (42)$$

$$\omega_r = \frac{\mathrm{P}}{j}\int (T_e - TL) \quad (43)$$

$$slip = \frac{(\omega - \omega r)}{\omega} \quad (44)$$

$$Power = \omega_r * T_e \quad (45)$$

SIMULATION OF EQUATIONS IN MATLAPP

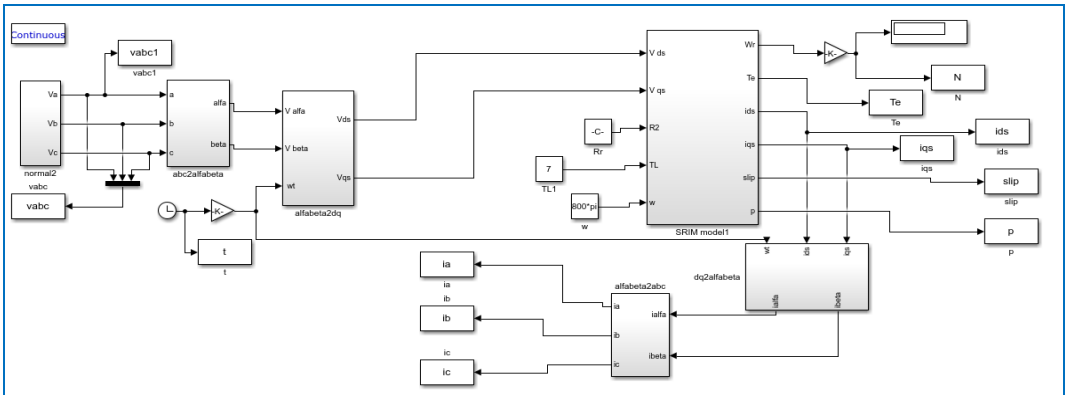

Fig. 9 simulation of overall operation parts of HS- SRIM

The general block of total simulation is showen in figure:

To clearify all parts of simulation starting with input abc to alphabeta to dq convertions Clarke –Park convertion :

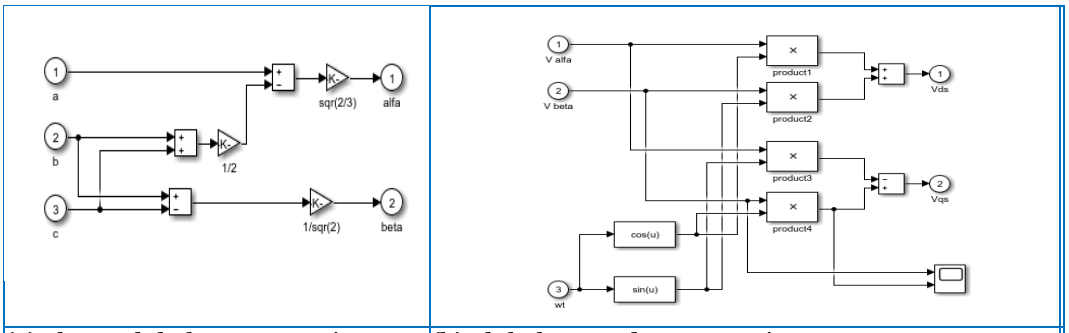

(a) abc to alphabeta convertion (b) alphabeta to dq0 convertion

Fig.10 input voltage convertions of SRIM part(eq 18 and 19)

The second block is SRIM MOTOR which contain the resultant equations(flux linkage,currents, torque,slip ,power ...etc)of model and it explained in figures below:

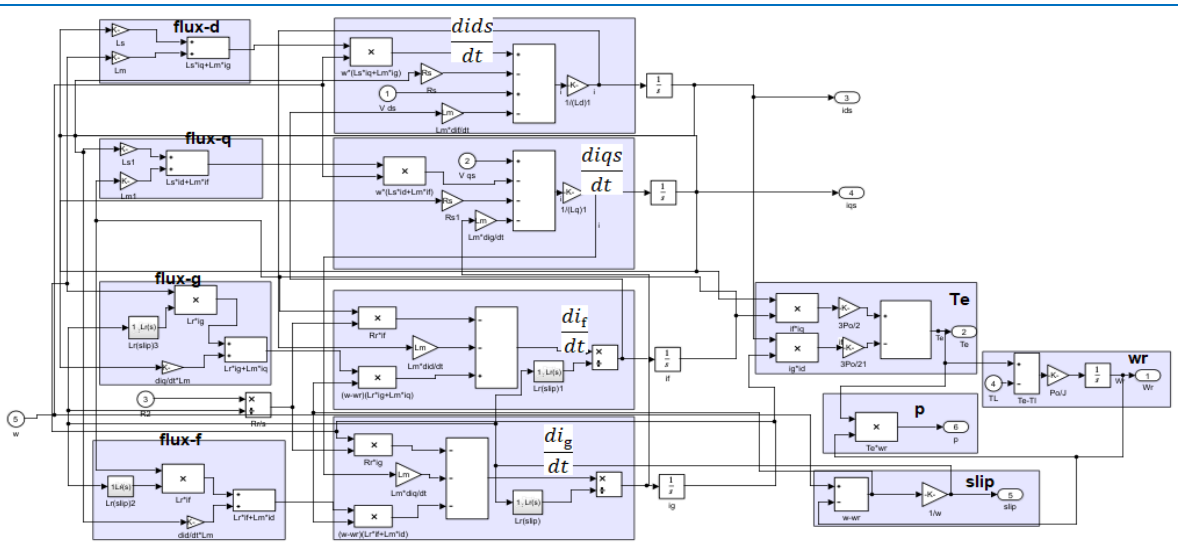

Fig. 11 simulation of SRIM motor block

The details of above figure representing the simulation of Eqs. (*34 – 37*) did/dt , diq/dt dif/dt and dig/dt in figures below :

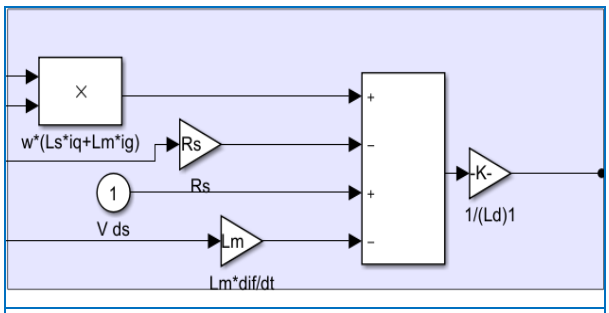

Fig. 12 simulation of Eqs. (*34*) did/dt

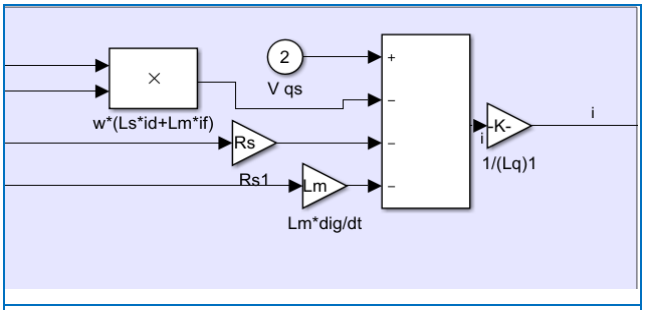

Fig. 13 simulation of Eqs. (*35*) diq/dt

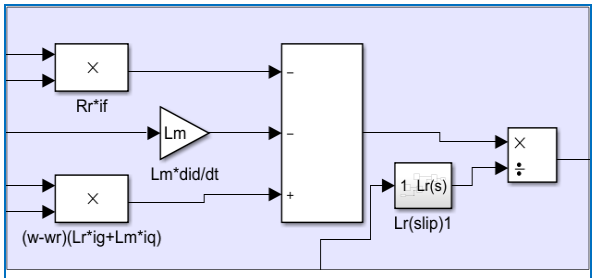

Fig. 14 simulation of Eqs. (*37*) dif/dt

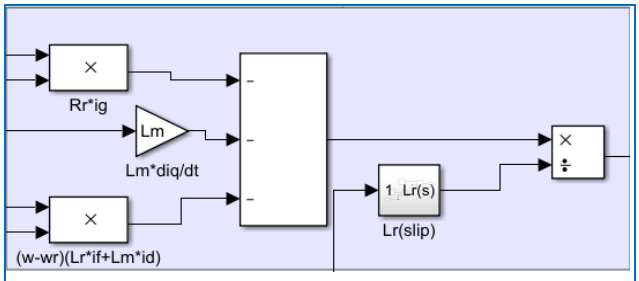

Fig.15 simulation of Eqs. (*36*) dig/dt

Equations (26-29) are simulated in the figures below:

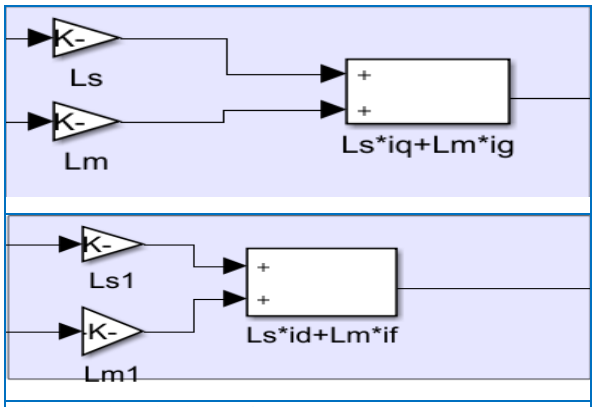

Fig. 16 simulation of λ_d *and* λ_q *equations* (*26 – 27*)

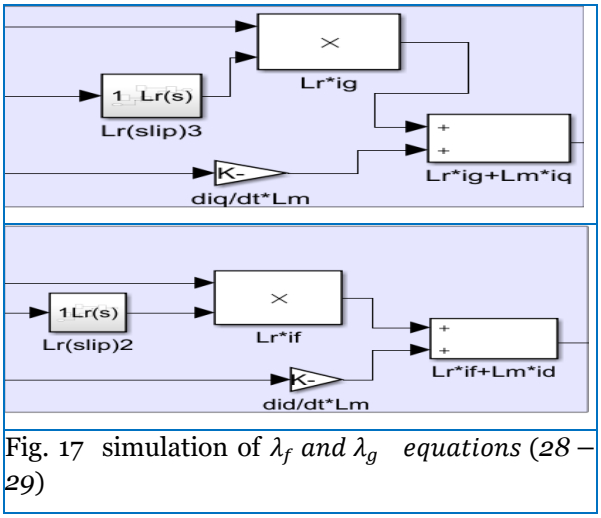

Fig. 17 simulation of λ_f *and* λ_g *equations* (*28 – 29*)

It can be seen that the rotor inductance is simulated as a function of slip configuration

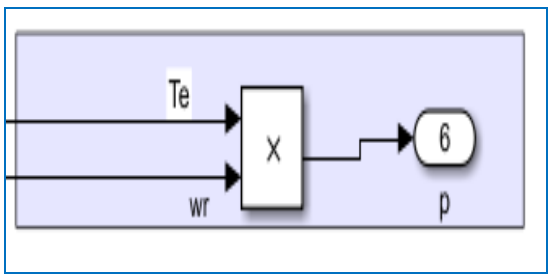

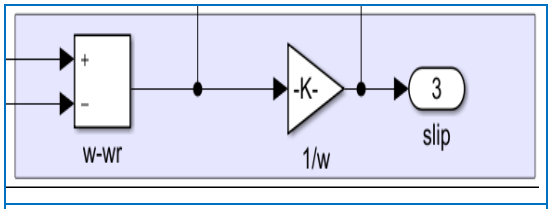

Fig.18 simulation of eqations (45-44) slip and electromagnetic power

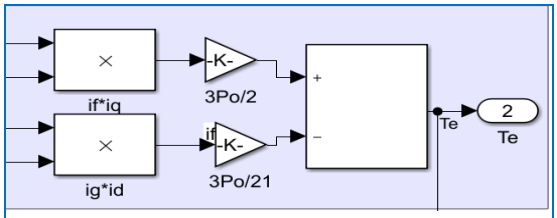

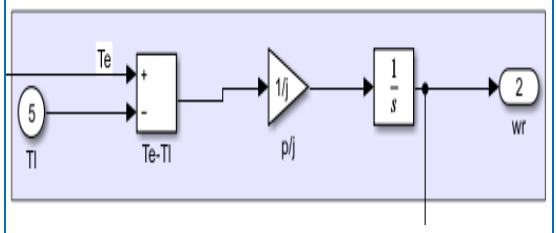

Fig. 19 simulation of eqations (42-43) torque and rotor speed

Output convertions dq to alphabeta to abc is showen in the figure below

.

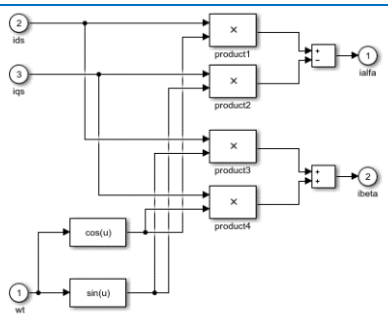

(a) dq to alphabeta convertion

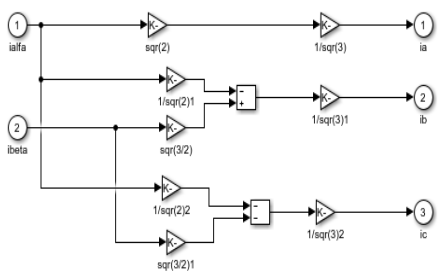

(b) alphabeta to abc convertion

Fig.(20) output current convertions part , eqs(20-21)

Results

Number of pole pairs, p	1
Number of phases, m	3
Number of stator slots, Q_S	24
Number of turns in series per phase of stator winding, N	14
Winding factor, k_w .	0.9577
Air gap, g/mm	0.75
Rotor diameter D/mm	98.5
Rotor length*/mm	100

Rated voltage U_s/V	225/130
rotor conductivity (σFe)	5*1000000 S/m
Rated current, I/A	65
Stator resistance, R/mΩ at 20C at 400 Hz	26
Srator leakage inductance, $L_{s\sigma}$/ μH	68.4

The rated frequency used in this model is 400 Hz and μ_{rs} is 40 Table 1 Motor Parameters

The result according to above parameters :

1- Under no load condition without putting end effect factor

2- Under full load condition without putting end effect factor

3- Under no load condition with end effect factor

4- Under full load condition with end effect factor

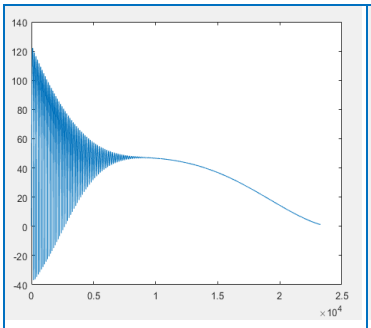

(a) *Te(N-m) vs N(rpm)*

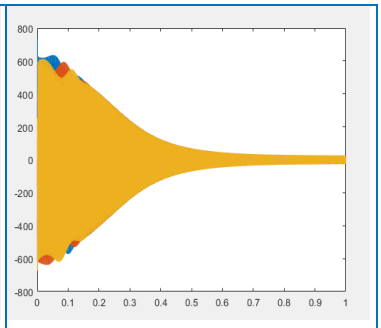

(b) Iabc(A) vs Time(sec)

Fig (21) torque and power

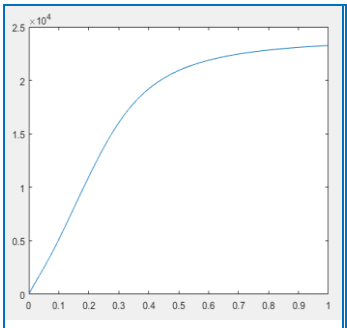

(a) *N vs Time*

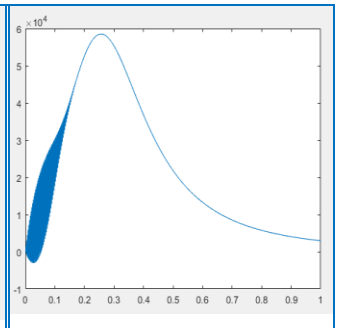

(b) p vs Time

Fig (22) speed and power

As explaind below:

1-No load no end effect factor

In fig(21) The transient period have highest torque value then steady state show the characteristics of solid rotor effect on torque curve verses rotor speed (a). Also the starting current at the same period then decreased during steady state period (b) in case of no load no end effect factor . At fig(22), no load no end effect factor it can be seen that the speed is approached to synchronous speed 24000 rpm (a) and the starting power reached to its maximum value then its decreased during the steady state

2-Full load-no end effect factor result.

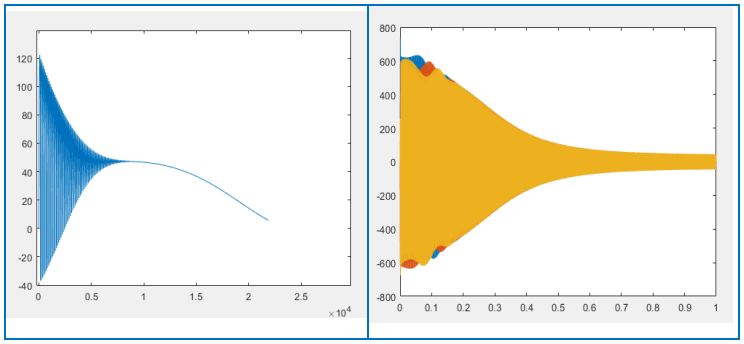

(a) *Te(N-m) vs N(rpm)*	(b) Iabc(A) vs Time(sec)

Fig (23) torque and power at full load

At fig (21) in full load case without end effect factor , the resultant torque slightly increased with the current as a result of adding the load during steady state and the speed get decreased because this load.

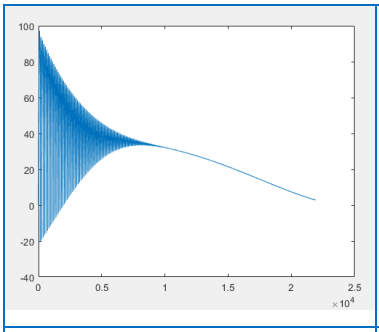

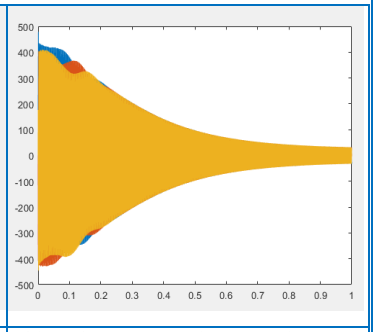

(a) *Te(N-m) vs N(rpm)*	(b) Iabc(A) vs Time(sec)

Fig (23) torque and power at no load(with end factor)

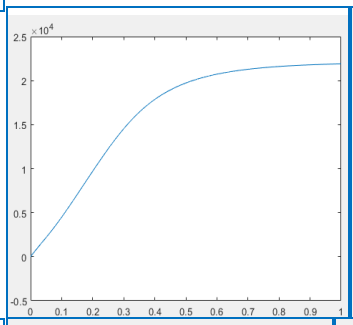

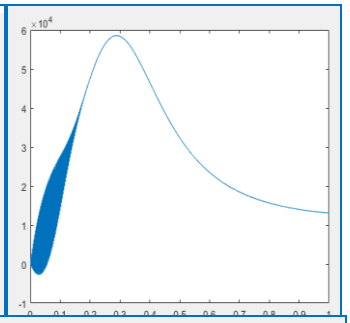

(a) *N vs Time*	(b) p vs Time

Fig (24) At no Load (with end factor)

At Fig 23 and 24, in no load case of adding the end effect factor , the resultant torque decreased , speed, decreased , the current and the power also decreased . the effect of the edge is clearly shown here.

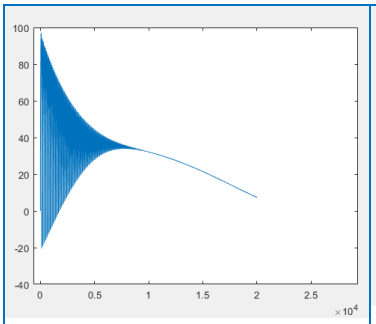

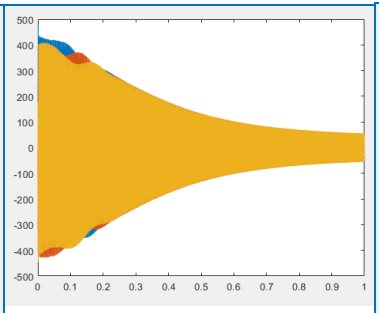

(a) *Te(N-m) vs N(rpm)*	(b) Iabc(A) vs Time(sec)

Fig (21) At full load (with end factor)

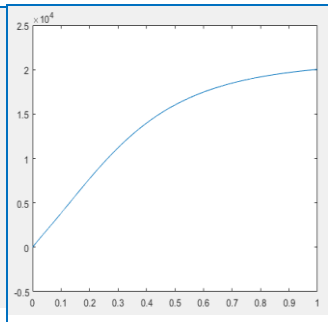

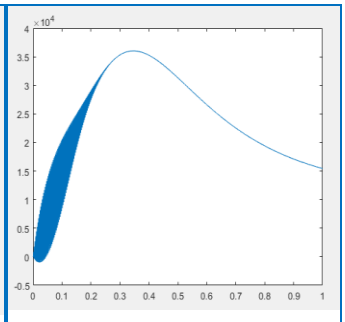

(a) *N vs Time*	(b) p vs Time

Fig (22) At full Load (without end factor)

At fig 15 at the case of full load with end effect factor , the increment of torque with the current and decrement of speed is clear.

5. CONCLUSIONS

The developed mathematical model successfully characterizes the dynamic behavior of high-speed solid rotor induction motors, incorporating rotor impedance derivations and dq-axis transformations to account for nonlinear material properties and edge effects. Simulations in MATLAB/Simulink highlight critical performance trends, including reduced torque and speed under edge effect conditions and the influence of load variations on transient responses. While the model demonstrates validity for the studied motor parameters, it reveals inherent inefficiencies at high operational frequencies (e.g., 400 Hz), necessitating further structural optimizations such as advanced rotor slotting or composite material integration. The inclusion of edge effect factors significantly refines accuracy, yet full 3D electromagnetic modeling remains essential for comprehensive design validation. Future research should

prioritize multi-physics simulations and experimental validation to bridge gaps between theoretical predictions and real-world performance, ultimately advancing HS-SRIM technology for industrial high-speed applications.

REFERENCES

[1] M. Mirzaei, "Computational Modeling of an Axial Airgap Induction Motor With a Solid Rotor," *IEEE Trans. Magn.*, vol. 58, no. 6, pp. 1–9, 2022, doi: 10.1109/TMAG.2022.3166962.

[2] C. Hong, W. Huang, and Z. Hu, "Calculation methods of equivalent circuit parameters for a dual stator solid rotor axial flux induction motor," *IET Renew. Power Gener.*, vol. 12, no. 16, pp. 1977–1983, Dec. 2018, doi: 10.1049/iet-rpg.2018.5103.

[3] H. Xu, J. Zhao, S. Yan, and H. Wang, "Magnetic field and rotor impedance analysis of solid rotor induction motors using the multilayer analytical method," *IET Electr. Power Appl.*, vol. 19, no. 1, 2025, doi: 10.1049/elp2.70004.

[4] B. Yan, X. Li, X. Wang, Y. Yang, and D. Chen, "Magnetic Field Prediction for Line-Start Permanent Magnet Synchronous Motor via Incorporating Geometry Approximation and Finite Difference Method Into Subdomain Model," *IEEE Trans. Ind. Electron.*, vol. 70, no. 3, pp. 2843–2854, 2023, doi: 10.1109/TIE.2022.3170621.

[5] H. Feng, X. Cui, J. Si, C. Gao, and Y. Hu, "Equivalent circuit model of novel solid rotor induction motor with toroidal winding applying composite multilayer theory," *Appl. Sci.*, vol. 9, no. 16, Aug. 2019, doi: 10.3390/app9163288.

[6] J. Xue *et al.*, "Modeling and Analysis of New Power Devices Based on Linear Phase-Shifting Transformer," *Processes*, vol. 10, no. 8, 2022, doi: 10.3390/pr10081596.

[7] T. Garbiec, M. Jagiela, and M. Kulik, "Application of Nonlinear Complex Polyharmonic Finite-Element Models of High-Speed Solid-Rotor Induction Motors," *IEEE Trans. Magn.*, vol. 56, no. 4, pp. 1–4, 2020, doi: 10.1109/TMAG.2019.2953987.

[8] R. P. Jastrzebski and A. K. Pilat, "Analysis of Unbalanced Magnetic Pull of a Solid Rotor Induction Motor in a Waste Heat Recovery Generator," *IEEE Trans. Energy Convers.*, vol. 38, no. 2, pp. 1208–1218, 2023, doi: 10.1109/TEC.2022.3227551.

[9] T.-Y. Lee, M.-K. Seo, Y.-J. Kim, and S.-Y. Jung, "Motor Design and Characteristics Comparison of Outer-Rotor-Type BLDC Motor and BLAC Motor Based on Numerical Analysis," *IEEE Trans. Appl. Supercond.*, vol. 26, no. 4, pp. 1–6, 2016, doi: 10.1109/TASC.2016.2548079.

[10] J. F. Gieras, J. Saari, and H. Sundstrand, "Performance Calculation for a High Speed Solid-Rotor Induction Motor."

[11] J. Pyrhönen, "The high-speed induction motor: Calculating the effects of solid-rotor material on machine characteristics," *Acta Polytech. Scand. Electr. Eng. Ser.*, vol. 68, 1991.

[12] J. Staszak, "Solid-Rotor Induction Motor Modeling Based on Circuit Model Utilizing Fractional-Order Derivatives," *Energies*, vol. 15, no. 17, Sep. 2022, doi: 10.3390/en15176371.

[13] D. Gerling and G. Dajaku, "Comparison of Different Calculation Methods for the Induction Motor with Multilayer Rotor Structure".

[14] A. T. Radhi and W. H. Zayer, "Faults diagnosis in stator windings of high speed solid rotor induction motors using fuzzy neural network," *Int. J. Power Electron. Drive Syst.*, vol. 12, no. 1, pp. 597–611, 2021, doi: 10.11591/ijpeds.v12.i1.pp597-611.

[15] C. A. C. Wengerkievicz, N. J. Batistela, N. Sadowski, T. Huguet, and Y. Lefèvre, "Experimental Loss Segregation in a Solid Rotor Induction Motor," *J. Microwaves, Optoelectron. Electromagn. Appl.*, vol. 21, no. 4, pp. 584–597, 2022, doi: 10.1590/2179-10742022v21i4268098.

[16] "POWER SYSTEM STABILITY Volume III Synchronous ~achines."

[17] P. Rathika and D. Devaraj, "Fuzzy Logic – Based Approach for Adaptive Hysteresis Band and DC Voltage Control in Shunt Active Filter," *Int. J. Comput. Electr. Eng.*, vol. 2, pp. 1793–8163, 2010, doi: 10.7763/IJCEE.2010.V2.169.

[18] T. Aho, V. Sihvo, J. Nerg, and J. Pyrhönen, "Rotor materials for medium-speed solid-rotor induction motors," in *Proceedings of IEEE International Electric Machines and Drives Conference, IEMDC 2007*, 2007, pp. 525–530. doi: 10.1109/IEMDC.2007.382722.